Imaging of closed cracks using nonlinear response of elastic waves at subharmonic frequency

doi: 10.1063/1.2426891

Imaging of closed cracks using nonlinear response of elastic waves at subharmonic frequency

Yoshikazu Ohara, Tsuyoshi Mihara, Ryouta Sasaki, Toshihiro Ogata, Setsu Yamamoto, Yuuki Kishimoto, and Kazushi Yamanaka[a)]
Department of Materials Processing, Tohoku University, Aoba 02, Sendai 980-8579, Japan

(Received 5 September 2006; accepted 28 November 2006; published online 2 January 2007)

The authors constructed a novel apparatus based on subharmonic ultrasound for the accurate imaging of closed cracks. Linear and nonlinear responses not only from the tip but also from other parts of cracks were observed in fundamental and subharmonic images, which were changed with varying closure stress. The subharmonic images always gave an accurate length of partially closed cracks, in contrast to the fundamental images in which the crack length was underestimated. Significant similarities in generation and resonance phenomena of subharmonic waves, acoustic emission, and the vibration of microbubbles are discussed. © *2007 American Institute of Physics*. [DOI: 10.1063/1.2426891]

Wave phenomena at interfaces between two media are important in many fields of science and technology. Among them, the scattering of elastic or electromagnetic waves at discontinuous interfaces in an elastic media, e.g., cracks, is applicable to safety inspection and hence has been extensively studied.[1,2] In particular, elastic waves are strongly scattered mostly at the tips or edges of a crack with an air gap between the crack faces ("open crack"), in which case cracks can be nondestructively detected.[3,4] However, elastic waves are transmitted through crack faces firmly pressed together owing to residual stress or by oxide films ("closed crack").[5–7] Conventional elastic wave inspection overlooks or underestimates closed cracks, which could result in catastrophic accidents.

Nonlinear response of elastic waves has a potential of becoming a primary means of detecting and evaluating closed cracks. In particular, subharmonic waves[7–14] with half frequency, which are generated at closed cracks irradiated with intense ultrasound, have a great selectivity of closed cracks.[11] However, the measurement of closed-crack length in thickness direction using subharmonic waves has not been performed. To achieve it, we constructed a novel imaging apparatus based on subharmonic waves and a phased array algorithm[15,16] (Fig. 1), which enables the accurate imaging of closed cracks. To irradiate cracks with the intense ultrasound required to generate subharmonic waves, we fabricated a $LiNbO_3$ single-crystal transmitter. As an input signal for the transmitter, we used a three-cycle tone burst of a 7 MHz sinusoidal wave. Although the particle displacement amplitude at a crack in an aluminum specimen can be larger than 20 nm, we set it at 10 nm, slightly above the subharmonic generation threshold. This is because there is a broad optimum range of input power for observing clear subharmonic resonance, as reported for bubbles in medical ultrasonic diagnosis.[17] As a receiver, an array sensor with a center frequency of 5 MHz was used for both fundamental and subharmonic components. To produce images, propagation times along the paths such as A-B-C-D in Fig. 1 were calculated and subtracted before the summation of signals received from each element of the array sensor. To filter the received signals at fundamental and subharmonic frequencies, digital bandpass filters were applied. Thus, the apparatus is able to selectively image closed and open cracks.

To verify the performance of the apparatus, we formed well-defined closed cracks in aluminum alloy (Al7075) specimens using a three-point bending fatigue test.[18,19] We also formed a closed crack in a stainless-steel specimen fabricated from the actual material (SUS316L) and had the actual thickness (40 mm) employed for the recirculation pipes of atomic power plants so as to simulate practical field testing. To control the closure stress, the maximum and minimum stress intensity factors during the fatigue test were set to those listed in Table I.

Figure 2 shows the fundamental and subharmonic images of cracks in the aluminum alloy specimens. In the high-

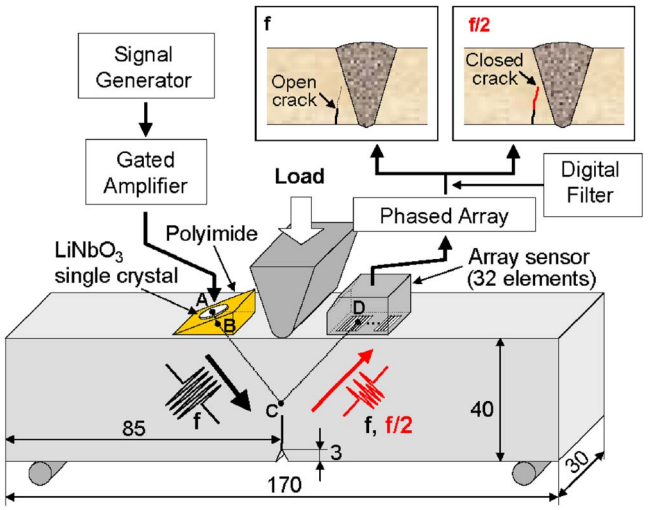

FIG. 1. (Color online) Experimental configuration of closed-crack imaging method using subharmonic waves. A is the center position of the $LiNbO_3$ single crystal, B is a passing point on the surface from A to the focal point C, which changes during scanning, and D is the position of an element of the array sensor. A-D are used to calculate propagation time in the specimen and wedge, depending on the elements of the array sensor. Fundamental (f) and subharmonic ($f/2$) components are extracted from received signals with digital filters and then fundamental and subharmonic images are created using each component. The schematic illustrations (upper right) are examples of fundamental and subharmonic images for a crack with a closed tip, e.g., in atomic power plants. The fundamental image will indicate only open parts. Hence, the crack length will be underestimated. On the other hand, the subharmonic image will indicate the accurate location of the crack tip.

[a)]Electronic mail: yamanaka@material.tohoku.ac.jp

TABLE I. Maximum and minimum stress intensity factors for fatigue test.

	Material	K_{max} (kgf/mm$^{3/2}$)	K_{min} (kgf/mm$^{3/2}$)
High-stress-intensity sample	Al7075	17	2
Low-stress-intensity sample	Al7075	14	2
Stainless-steel sample	SUS316L	60	2

stress-intensity sample, the crack tip was clearly observed in the fundamental image [Fig. 2(a)], whereas it was invisible in the subharmonic image [Fig. 2(b)]. This result shows that the crack tip was open. It was also confirmed that the location of the crack tip in the obtained image agreed with that of the actual crack tip on the sidewall shown in the photograph [Fig. 2(c)]. In contrast, in the low-stress-intensity sample, the crack tip was invisible in the fundamental image [Fig. 2(d)], whereas it was clearly observed in the subharmonic image [Fig. 2(e)]. This result shows that the crack tip was partially closed. Thus, we demonstrated that the subharmonic image indicates the accurate location of closed cracks.

After confirming the performance of the apparatus, we applied it to a model of a critical component of an atomic power plant (stainless-steel sample in Table I) and examined the change in crack images with varying crack closure stress by changing the nominal bending stress induced by a static load (Fig. 1). Here, nominal bending stress was calculated from the applied load, elastic properties, density, and geometry under the condition of a crack-free beam. The nominal bending stress is a measure of the stress relieved from the closure stress, although the rigorous calculation of the closure stress is difficult owing to the complexity of the stress field around the crack. The fundamental and subharmonic images under the nominal bending stresses of 19, 84, and 112 MPa and schematic illustrations for the interpretation of those images are shown in Fig. 3.

When the bending stress was 19 MPa, the fundamental image [Fig. 3(a)] indicated only the notch part C. This result suggests that the boundary between the notch and the closed crack had a distinct discontinuity and thus C became a linear scattering source. On the other hand, the subharmonic image [Fig. 3(b)] indicated not only C but also the crack tip A and the middle part B. This result shows that the present apparatus is able to image various parts of the crack, including the tip.

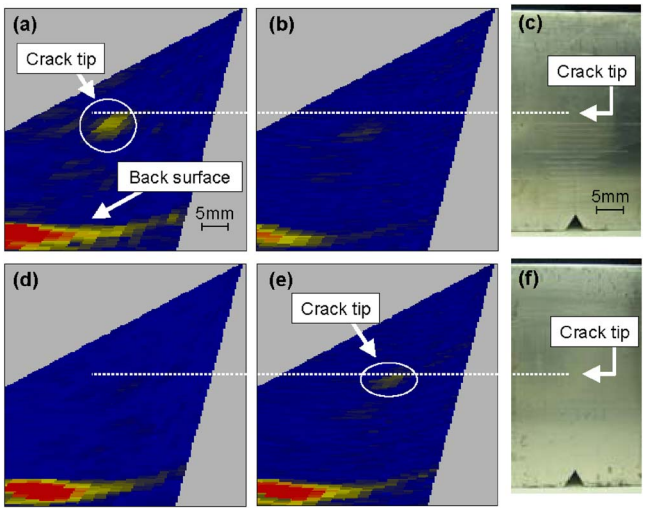

FIG. 2. (Color online) Comparison of crack tip images obtained by developed imaging apparatus with actual fatigue cracks of high- and low-stress-intensity samples of Al7075. [(a), (b), and (c)] Fundamental image, subharmonic image, and photograph of high-stress-intensity sample, respectively. [(d), (e), and (f)] Fundamental image, subharmonic image, and photograph of low-stress-intensity sample, respectively.

When the bending stress was 84 MPa, the fundamental image [Fig. 3(d)] indicated only the middle part B. This result shows that B was a distinct boundary between the open and closed regions and thus B became a linear scattering source. The subharmonic image [Fig. 3(e)] indicated both A and B, although the intensity at B decreased in comparison with that in Fig. 3(b). This result shows that the present apparatus is able to image the crack tip, irrespective of the closure stress.

When the bending stress was 112 MPa, no part of the crack was observed in the fundamental image [Fig. 3(g)]. It is surprising that the indication of B observed in Fig. 3(d) was lost, even though the crack was more open. This result is understood by assuming that the boundary between the open and closed regions at B became ambiguous with the increase in bending stress, and therefore the linear scattering source diminished. In contrast, the subharmonic image [Fig. 3(h)] indicated A. This result shows that A was still closed, which

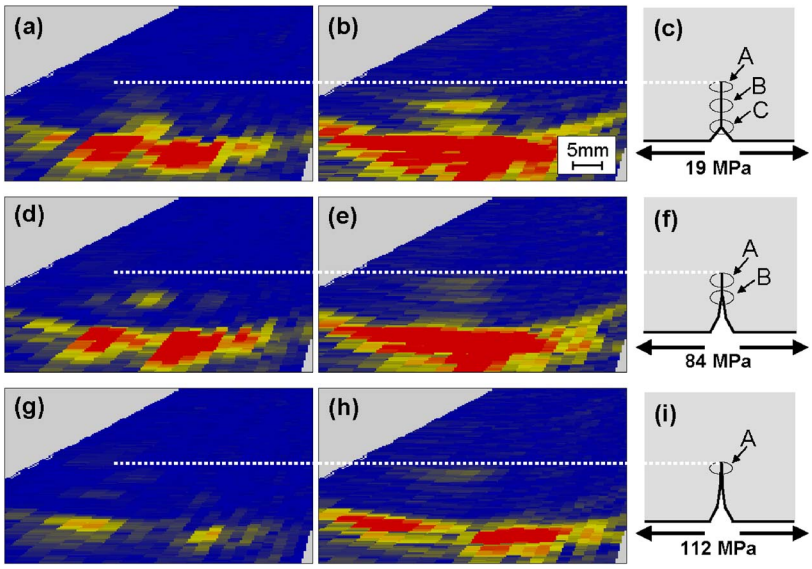

FIG. 3. (Color online) Dependence of crack images with varying static bending stress in fatigue crack of SUS316L. [(a) and (b)] Fundamental and subharmonic images, respectively, for nominal bending stress of 19 MPa. (c) Schematic illustration for interpretation of (a) and (b). [(d) and (e)] Fundamental and subharmonic images, respectively, for nominal bending stress of 84 MPa. (f) Schematic illustration for interpretation of (d) and (e). [(g) and (h)] Fundamental and subharmonic images, respectively, for nominal bending stress of 112 MPa. (i) Schematic illustration for interpretation of (e) and (f). In (c), (f), and (i), A–C denote the crack tip, middle part, and notch part, respectively, which are fundamental and/or subharmonic scattering sources.

is favorable for subharmonic generation. The most striking finding in the above results is that the crack had a markedly high residual stress that was only partly relieved by applying the nominal maximum bending stress of more than 100 MPa. Nevertheless, note that we successfully imaged the change in crack state with varying closure stress and that the subharmonic images always gave an accurate crack length, in contrast to the fundamental images in which the crack length was underestimated. Thus, the developed imaging apparatus will improve inspection techniques to satisfy the reliability requirements of materials and structural components in atomic power plants.

In addition to the immediate implication reported above, the present findings have further implications. Acoustic emission (AE),[20–23] which is generated at various parts of cracks in the initiation and propagation stages, has been used for material evaluation in the field of material science and safety science. There are significant similarities between subharmonic waves and AE. They are both generated at various parts of crack faces, since the generation is caused by a contact or rubbing of crack asperity.[20–22] On the other hand, it was reported that an AE signal has a dominant frequency that depends on the crack length and elastic properties and involves subharmonic components under an appropriate condition[23] caused by the resonance of Rayleigh waves propagating on the crack face.[24] We pointed out that subharmonic generation at closed cracks is caused by the resonance of Rayleigh waves on the crack faces.[12] Also, the condition for the generation of an AE signal involving subharmonic components is that the initial displacement of the crack face induced by the external load increases above a certain threshold.[23] The threshold behavior of subharmonic generation at closed cracks has been experimentally[7–10,13] and theoretically[13] studied. These are interesting similarities between subharmonic waves and AE. Since subharmonic generation is repeatable whereas AE is not, a precise examination of subharmonic generation using our apparatus would be helpful for the further understanding of the AE generation mechanism and for an improvement in inverse-problem analysis.[22]

There are also interesting similarities between subharmonic waves generated at closed cracks and the vibration of microbubbles. In medical diagnosis, the vibration of microbubbles including subharmonic resonance has been extensively studied to improve ultrasonic contrast.[17,25,26] The accumulated knowledge should be transferred to the field of crack diagnosis for the further understanding of subharmonic resonance at closed cracks. On the other hand, observation of images or accurate wave forms of microbubbles requires levitation and trapping by the acoustic radiation pressure,[27,28] whereas that of cracks does not. Accordingly, relation between sources of subharmonics can be more precisely studied in cracks, as shown in Fig. 3. The similarities and differences between microbubbles and cracks will be an interesting subject which will provide further progress in these fields.

The images of the closed-crack parts were observed as wide areas, rather than lines due to the low lateral resolution limited by small aperture size of the array. However, the lateral resolution can be improved by increasing the aperture size, together with increasing the number of elements, e.g., from 32 to 128 elements, to avoid grating lobe formation.[29,30]

The weld parts schematically shown in Fig. 1 would distort both fundamental and subharmonic images because of their strong anisotropy as a general problem in ultrasonic nondestructive evaluation. Also, fundamental images would be attenuated since the weld parts are strong linear scattering sources. However, we expect that subharmonic images are still useful to detect closed cracks because subharmonic waves are generated only at closed cracks, and the attenuation is much lower than that of the fundamental waves.

This work was supported by Grants-in-Aid for Science Research (Nos. 16206071 and 174727) from the Ministry of Education, Culture, Sports, Science and Technology of Japan, and by Japan Nuclear Energy Safety Organization.

[1] L. D. Landau and E. M. Lifshitz, *Theory of Elasticity* (Pergamon, Oxford, 1986), p. 87.
[2] M. Born and E. Wolf, *Principles of Optics: Electromagnetic Theory of Propagation, Interference and Diffraction of Light* (Pergamon, Oxford, 1980), p. 556.
[3] L. W. Schmerr, *Fundamentals of Ultrasonic Nondestructive Evaluation* (Plenum, New York, 1998), p. 305.
[4] J. D. Achenbach, Int. J. Solids Struct. **37**, 13 (2000).
[5] O. Buck, W. L. Morris, and J. M. Richardson, Appl. Phys. Lett. **33**, 371 (1978).
[6] Y. Zheng, R. G. Maev, and I. Y. Solodov, Can. J. Phys. **77**, 927 (1999).
[7] I. Y. Solodov and C. A. Vu, Acoust. Phys. **39**, 476 (1993).
[8] I. Y. Solodov, N. Krohn, and G. Busse, Ultrasonics **40**, 621 (2002).
[9] A. Moussatov, V. Gusev, and B. Castagnede, Phys. Rev. Lett. **90**, 124301 (2003).
[10] I. Y. Solodov, J. Wackerl, K. Pfleiderer, and G. Busse, Appl. Phys. Lett. **84**, 5386 (2004).
[11] K. Yamanaka, T. Mihara, and T. Tsuji, Jpn. J. Appl. Phys., Part 1 **43**, 3082 (2004).
[12] K. Yamanaka, R. Sasaki, T. Ogata, Y. Ohara, and T. Mihara, in *Review of Progress in Quantitative Nondestructive Evaluation*, edited by D. O. Thompson and D. E. Chimenti (Plenum, New York, 2006), Vol. 25, pp. 291–298.
[13] Y. Ohara, T. Mihara, and K. Yamanaka, Ultrasonics **44**, 194 (2006).
[14] R. Sasaki, T. Ogata, Y. Ohara, T. Mihara, and K. Yamanaka, Jpn. J. Appl. Phys., Part 1 **44-6B**, 4389 (2005).
[15] E. P. Papadakis, *Ultrasonic Instruments & Devices: Reference for Modern Instrumentation, Techniques, and Technology* (Academic, New York, 2000), p. 102.
[16] T. L. Szabo, *Diagnostic Ultrasound Imaging: Inside Out* (Academic, New York, 2004), p. 171.
[17] P. Palanchon, A. Bouakaz, J. Klein, and N. D. Jong, Ultrasound Med. Biol. **29**, 417 (2003).
[18] M. Akino, T. Mihara, and K. Yamanaka, in *Review of Progress in Quantitative Nondestructive Evaluation*, edited by D. O. Thompson and D. E. Chimenti (Plenum, New York, 2004) Vol. 23, pp. 1256–1263.
[19] J.-Y. Kim, V. A. Yakovlev, and S. I. Rokhlin, Appl. Phys. Lett. **82**, 3203 (2003); J. Acoust. Soc. Am. **115**, 1961 (2004).
[20] A. Berkovits and D. Fang, Eng. Fract. Mech. **51**, 401 (1995).
[21] A. Guarino, A. Garcimartin, and S. Ciliberto, Eur. Phys. J. B **6**, 13 (1998).
[22] T. Kishi, Mater. Trans. **44**, 1546 (2003).
[23] V. V. Krylov, P. S. Landa, and V. A. Robsman, Acoust. Phys. **39**, 55 (1993).
[24] D. E. Budreck and J. D. Achenbach, J. Appl. Mech. **55**, 405 (1988).
[25] P. M. Shankar, P. D. Krishna, and V. L. Newhouse, J. Acoust. Soc. Am. **106**, 2104 (1999).
[26] P. D. Krishna, P. M. Shankar, and V. L. Newhouse, Phys. Med. Biol. **44**, 681 (1999).
[27] T. J. Asaki, P. L. Marston, and E. H. Trinh, J. Acoust. Soc. Am. **93**, 706 (1993).
[28] E. H. Trinh, D. B. Thiessen, and R. G. Holt, J. Fluid Mech. **364**, 253 (1998).
[29] S. Wooh and Y. Shi, Wave Motion **29**, 245 (1999).
[30] S. Wooh and Y. Shi, J. Nondestruct. Eval. **18**, 39 (1999).